Heating Characteristics of Thin Helical Antennas with Conducting Cores in a Lossy Medium—I: Noninsulated Antennas

Mark S. Mirotznik, *Member, IEEE,* Nader Engheta, *Senior Member, IEEE,* and Kenneth R. Foster, *Fellow, IEEE*

***Abstract*—We report a combined theoretical and experimental study of the heating characteristics of helical antennas in lossy dielectric media. Proposed biomedical application of such antennas include angioplasty, hyperthermia, and catheter ablation of tissue. The study focuses on helical antennas, operated in the normal mode (wavelength greater than antenna diameter but comparable to antenna length), that are terminated at one end by a short circuit and at the other by a coaxial feedpoint. The analytical model is based on the helical sheath approximation, extended to the case of lossy media. In addition, experimental studies were performed on helical antennas immersed in aqueous electrolyte of various conductivity. The antennas show two distinct modes of propagation: a slow mode similar to that observed in helical antennas in loss-free media, and a faster mode. The analytical/numerical results are in good agreement with experimental data, thus demonstrating the validity of the model.**

I. Introduction

HELICAL antennas are well known for their applications in communications, where they are typically employed in their endfire mode. Quite a different application involves their use for heating, using long, thin antennas immersed in the media to be heated. Proposed biomedical applications of such antennas include angioplasty, catheter ablation of tissue [1], and hyperthermia [2]–[4].

Little work has been done to analyze the heating characteristics of such helical antennas in lossy media, and most previous reports are experimental in nature. Satoh *et al.* [2], [3] and Wu *et al.* [4] described the heating patterns of several helical antennas used as interstitial hyperthermia applicators; they did not present a comprehensive theoretical or numerical analysis of the antenna characteristics as functions of helical pitch or other design parameters. The important issues include the depth of heating and uniformity of heating along the length of the antenna. There is a need for more general analysis of such antennas, to describe their characteristics as functions of antenna geometry and dielectric properties of the medium.

Manuscript received April 13, 1992; revised November 30, 1992. The work of N. Engheta was supported by the National Science Foundation under PYI Account ECS-8957434.

M. S. Mirotznik is with the Department of Electrical Engineering, The Catholic University of America, Washington, DC 20064.

N. Engheta is with the Department of Electrical Engineering, University of Pennsylvania, Philadelphia, PA 19104-6390.

K. R. Foster is with the Department of Bioengineering, University of Pennsylvania, Philadelphia, PA 19104–6392.

IEEE Log Number 9210223.

There is a considerable amount of literature relevant to the helical antenna. However, due to the complicated boundary conditions imposed by the actual wire wound helix, all previous studies have relied on approximate models. One such model, originally studied by Sensiper [5], approximated the actual wire wound helix by an anisotropically conducting sheath. Sensiper obtained the field distributions and dispersion characteristics assuming the antennas were radiating into free space. The antennas studied by Sensiper did not include an inner core and were assumed to be infinite in length.

Neureuther *et al.* [6] extended Sensiper's model to include a conducting core (the case of interest here). He also studied a more physically realistic, but mathematically difficult, model consisting of a perfectly conducting spiral tape, and showed that the sheath model was a good approximation. Neureuther *et al.,* like Sensiper, assumed the antennas were radiating into free space and were infinite in length. Perini [7] carried out an extensive theoretical and experimental study of helical antennas. He used a spiral tape model with conducting core to compare calculated results to experimental measurements. He was primarily concerned with the antenna's radiation pattern and, consequently, only considered antennas radiating into free space.

More recently, Hill and Wait [8] carried out an elegant theoretical study on wave propagation along coaxial cables with helical shields. Their model consisted of a dielectric coated conductor which was shielded by a finite number of helices. Utilizing a modal expansion technique, they solved for the propagation characteristics of waves traveling along their antennas. They were particularly interested in the leaky feeder technique used to provide radio communication in mine tunnels. Although that is quite different from the application of interest here, the method used by Hill and Wait is utilized in this work.

Only a few investigators have studied the helical antenna immersed in a lossy medium, and these studies have been numerical in nature. Chen [9] developed an integral equation for an infinite length helical sheath antenna radiating into a lossy medium. His equations could then be solved numerically for the antenna's current distribution. Casey and Bansal [10] extended Chen's work to the case of a finite length helical sheath antenna in a general lossy medium. In addition, they developed a numerical method based on the moment method for solving their integral equation. The antennas considered

by these investigators did not include a dielectrically coated inner conductor or the effects of a coaxial feedpoint and short circuit termination, as is the case here. However, the solutions reported by Casey and Bansal were used to check limiting cases for the model presented in this work.

The model presented in this paper extends the analytical work of Hill and Wait, Neureuther *et al.*, Sensiper, and others to include the effects of a coaxial feedpoint, a short circuit termination, and an external *lossy* medium. These considerations, which are necessary for the present application of microwave catheter ablation, have not, to the best of our knowledge, been studied by any previous investigator of helical antennas.

In this paper, we first present an analytical antenna model for the helical sheath antenna immersed in lossy media. We then extend the analysis to include a coaxial feedpoint and a short circuit termination. Finally, the results from the analytical antenna model are compared to experimental results.

II. Antenna Model

A typical insulated helical antenna [11] for biomedical applications is shown in Fig. 1. This antenna is fabricated from a coaxial transmission line with inner and outer conductors of radii a and b, separated by a (loss-free) dielectric medium of permittivity ε_1 and permeability μ_o. At the end of this transmission line, the other conductor is stripped back for a distance L and the helical antenna placed over the line. The antenna is connected at the distal end to the inner conductor of the coaxial line, and at the proximal end to the outer conductor of the transmission line. Thus, the antenna has length L, and in this arrangement it is terminated at one end by the coaxial feedpoint, and at the other by a short circuit. The medium outside the helical wire is taken to infinite in extent, lossy but nonmagnetic, with parameters $\varepsilon_2 = \varepsilon_2' - j\varepsilon_2''$, and μ_o.

Following the approach of Sensiper, we model the helical antenna in cylindrical coordinates (ρ, ϕ, z) by a sheath helix, i.e., an anisotropically conducting cylindrical tube (Fig. 2). The sheath is assumed to be perfectly conducting in a direction making an angle α with the plane perpendicular to the axis of the antenna, and perfectly insulating normal to this direction. The short circuit termination is modeled by a perfectly conducting cap at the end of the antenna.

III. Formulation

To determine the fields present in the inside and outside the dielectric media, a modal expansion technique is utilized. This method is based on the technique used by Hill and Wait [8], Casey [10], Lee [12], and others in treating loosely braided coaxial cables with helical shields.

The electric and magnetic fields in the regions internal and external to the helical sheath (represented by subscripts 1 and 2, respectively) are constructed using the electric and magnetic Hertz vectors $\tilde{\Pi}^e$ and $\tilde{\Pi}^m$, respectively. For a waveguide whose cross section is uniform along the z direction, it has been shown that a general solution to Maxwell's equation can be found from only the z components of these vectors [13].

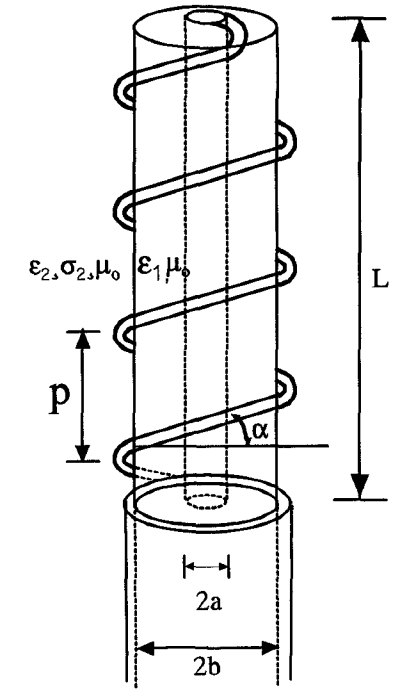

Fig. 1. Helical antenna of length L, outer radius b, inner radius a, helical pitch angle α, and pitch p, immersed in an external lossy media.

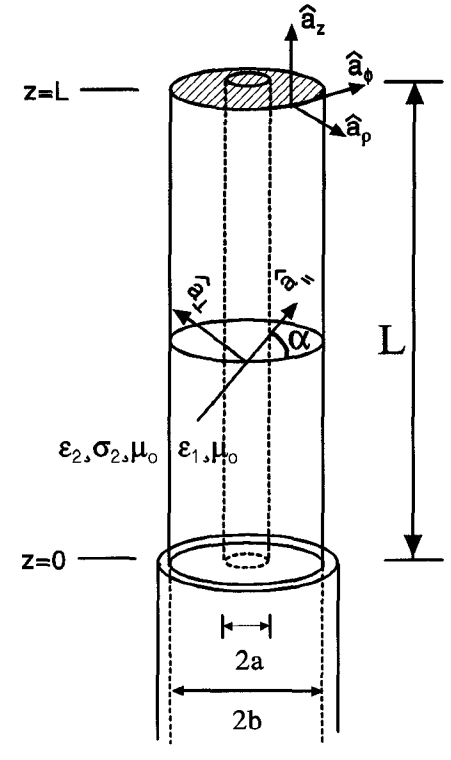

Fig. 2. Helical sheath model of length L, outer radius b, inner radius a, helical pitch angle α, immersed in an external lossy media. Sheath model defined as anisotropically conducting thin cylinder, which is perfectly conducting at an angle, α, w.r.t. horizontal axis and perfectly insulating normal to that direction. Perfectly conducting cap provides short circuit termination.

Thus, in each region,

$$\tilde{E} = -j\omega\mu_o \nabla \times \tilde{\Pi}^m + \left(k^2 + \nabla\nabla\cdot\right)\tilde{\Pi}^e$$
$$\tilde{H} = j\omega\varepsilon \nabla \times \tilde{\Pi}^e + \left(k^2 + \nabla\nabla\cdot\right)\tilde{\Pi}^m \quad (1)$$

where ω is the angular frequency, k is the wavenumber in the internal $\left(k_1 = \left(\omega\sqrt{(\mu_o\varepsilon_1)}\right)\right)$ or external $\left(k_2 = \left(\omega\sqrt{(\mu_o\varepsilon_2)}\right)\right)$ regions, $\tilde{\Pi}^e = \Pi_z^e\hat{z}$ and $\tilde{\Pi}^m = \Pi_z^m\hat{z}$. All field quantities vary with time according to $e^{j\omega t}$.

The z component of the Hertzian vector potential satisfies the scalar Helmholtz equations in each region

$$\begin{aligned}\left(\nabla^2 + k^2\right)\Pi_z^e &= 0\\ \left(\nabla^2 + k^2\right)\Pi_z^m &= 0\end{aligned} \tag{2}$$

with the appropriate boundary conditions. There are several solutions for Π_z^e and Π_z^m for this equation. The total solution can thus be written as the linear superposition of these solutions

$$\begin{aligned}\Pi_z^e(\rho,\phi,z) &= \sum_n\sum_p \Pi_{n,p}^e(\rho)e^{-j\beta_{n,p}z}e^{-jn\phi}\\ \Pi_z^m(\rho,\phi,z) &= \sum_n\sum_p \Pi_{n,p}^m(\rho)e^{-j\beta_{n,p}z}e^{-jn\phi}\end{aligned} \tag{3}$$

where n and p represent variations in the azimuthal and radial directions, respectively.

The boundary conditions for the electric and magnetic fields at $\rho = b$ are

$$\begin{aligned}E_z^{n,p}(b)_1 &= E_z^{n,p}(b)_2\\ E_\phi^{n,p}(b)_1 &= E_\phi^{n,p}(b)_2\\ H_z^{n,p}(b)_1 &= H_z^{n,p}(b)_2 + j_\phi^{n,p}\\ H_\phi^{n,p}(b)_1 &= H_\phi^{n,p}(b)_2 - j_z^{n,p}\end{aligned} \tag{4}$$

where $j_z^{n,p}$ and $j_\phi^{n,p}$ represent the z and ϕ components of the surface current density for the (n,p) mode, and the superscripts n and p denote the field components derived from the corresponding mode of $\Pi_{n,p}^e$ and $\Pi_{n,p}^m$. The boundary conditions at $\rho = a$ are

$$E_z^{n,p}(a) = E_\phi^{n,p}(a) = 0\,. \tag{5}$$

After solving (2) and matching the boundary conditions given above, the general solutions can be obtained as given by Hill and Wait [8].

We are assuming in this case that the helical antennas are being driven by a coaxial line source (with its dominant mode), in which the electric and magnetic source fields are independent of azimuthal angle ϕ. Due to this symmetry in the coaxial line source, and since the antennas are electrically thin ($2\pi b << \lambda$), it can be assumed that the $n = 0$ modes are of interest here. For these modes, the solutions reduce to the following expressions as given in [8]: (see (6) and (7) at bottom of page)
where

$$\begin{aligned}u_o &= \sqrt{\beta_o^2 - k_1^2}, \qquad \nu_o = \sqrt{\beta_o^2 - k_2^2}\\ Z_o(u_o\rho) &= I_o(u_o\rho) - \frac{I_o(u_oa)}{K_o(u_oa)}K_o(u_o\rho)\\ Z_o^*(u_o\rho) &= I_o(u_o\rho) - \frac{I_o'(u_oa)}{K_o'(u_oa)}K_o(u_o\rho)\end{aligned} \tag{8}$$

where $\beta_o \triangleq \beta_{o,p}$ and I_o and K_o are the modified Bessel functions of the first and second kind, and the prime refers to a derivative with respect to the entire argument. The constants A_o, A_o^*, B_o, B_o^* are given

$$\begin{aligned}A_o &= \frac{jI_tu_oZ_o(u_ob)\sin(\alpha)}{2\pi b\omega\nu_o[\epsilon_2K_o'(\nu_ob)Z_o(u_ob)u_o - \epsilon_1K_o(\nu_ob)Z_o'(u_ob)\nu_o]}\\ A_o^* &= \frac{I_tZ_o^{*\prime}(u_ob)\cos(\alpha)}{2\pi b\nu_o[K_o'(\nu_ob)Z_o^{*\prime}(u_ob)\nu_o - K_o'(\nu_ob)Z_o^*(u_ob)u_o]}\\ B_o &= \frac{jI_t\nu_oK_o(\nu_ob)\sin(\alpha)}{2\pi b\omega u_o[\epsilon_2K_o'(\nu_ob)Z_o(u_ob)u_o - \epsilon_1K_o(\nu_ob)Z_o'(u_ob)\nu_o]}\\ B_o^* &= \frac{I_tK_o'(\nu_ob)\cos(\alpha)}{2\pi bu_o[K_o'(\nu_ob)Z_o^{*\prime}(u_ob)\nu_o - K_o'(\nu_ob)Z_o^*(u_ob)u_o]}\end{aligned} \tag{9}$$

where $I_t = 2\pi bj_z/\sin(\alpha) = 2\pi bj_\phi/\cos(\alpha)$ is the total surface current of the $n = 0$ mode [8]. The relations given above for $n = 0$ are true for all modes with radial variation p; but for convenience, the subscript p has been omitted.

IV. Dispersion Characteristics

A dispersion relationship between the propagation constant β_o and free-space wavenumber k $\left(= \omega\sqrt{\varepsilon_o\mu_o}\right)$ can be derived from the boundary condition that the electric field component on the helical sheath in the direction α must vanish.

$$\frac{\omega^2\mu_o\cos(\alpha)^2}{\frac{K_o(\nu_ob)}{K_o'(\nu_ob)}\nu_o^2 - \frac{Z_o^*(u_ob)}{Z_o^{*\prime}(u_ob)}u_o\nu_o} - \frac{\mu_o\sin(\alpha)^2}{\epsilon_2\frac{K_o'(\nu_ob)}{K_o(\nu_ob)}u_o - \epsilon_1\frac{Z_o'(u_ob)}{Z_o(u_ob)}\nu_o} = 0\,. \tag{10}$$

The propagation constant β_o, which may be complex in general, can be calculated by determining the roots of the above equation. For the special case where the inner and outer media are identical, this dispersion relation reduces to that

$$\rho > b$$

$$\begin{aligned}E_\rho &= -j\beta_o\nu_oA_oK_o'(\nu_o\rho)e^{-j\beta_oz} & H_\rho &= -j\beta_o\nu_oA_o^*K_o'(\nu_o\rho)e^{-j\beta_oz}\\ E_\phi &= j\mu_o\omega\nu_oA_o^*K_o'(\nu_o\rho)e^{-j\beta_oz} & H_\phi &= -j\omega\epsilon_2\nu_oA_oK_o'(\nu_o\rho)e^{-j\beta_oz}\\ E_z &= -\nu_o^2A_oK_o(\nu_o\rho)e^{-j\beta_oz} & H_z &= -\nu_o^2A_o^*K_o(\nu_o\rho)e^{-j\beta_oz}\end{aligned} \tag{6}$$

$$a < \rho < b$$

$$\begin{aligned}E_\rho &= -j\beta_ou_oB_oZ_o'(u_o\rho)e^{-j\beta_oz} & H_\rho &= -j\beta_ou_oB_o^*Z_o^{*\prime}(u_o\rho)e^{-j\beta_oz}\\ E_\phi &= j\mu_o\omega u_oB_o^*Z_o^{*\prime}(u_o\rho)e^{-j\beta_oz} & H_\phi &= -j\omega\epsilon_1u_oB_oZ_o'(u_o\rho)e^{-j\beta_oz}\\ E_z &= -u_o^2B_oZ_o(u_o\rho)e^{-j\beta_oz} & H_z &= -u_o^2B_o^*Z_o^*(u_o\rho)e^{-j\beta_oz}\end{aligned} \tag{7}$$

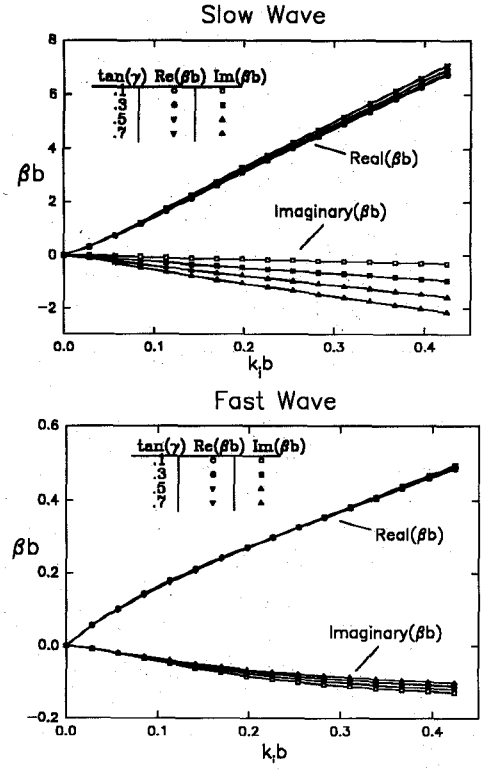

Fig. 3. Slow and fast wave $k_1 b - \beta b$ diagram ($k_1 = \omega\sqrt{(\mu_o \varepsilon_1)}$ for $b/a = 2.0$, $n = 0$, helical pitch angle $\alpha = 15°$, $\varepsilon_2'/\varepsilon_1' = 30$ and the loss tangent, $\tan(\gamma) = \varepsilon_2''/\varepsilon_2'$, is varied from 0.1 to 0.7.

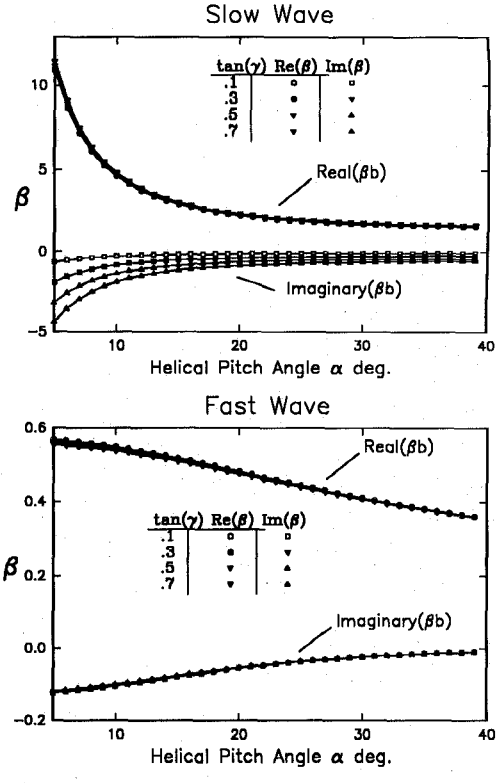

Fig. 4. Slow and fast wave propagation constant vs. helical pitch angle for $f = 915$ MHz, $b = 0.1$ cm, $a = 0.05$ cm, $\varepsilon_2'/\varepsilon_1' = 30$ with $\varepsilon_1' = 2$ and loss tangent, $\tan(\gamma) = \varepsilon_2''/\varepsilon_2'$, is varied from 0.1 to 0.7.

earlier reported in [5]. In considering the present results, we distinguish between antennas in lossy and lossless media; only the latter case was discussed in [5].

Lossless Media: In this case, for the lowest order guided mode of $n = 0$ and for the parameters used in our problem, the propagation constants β_o are real, and greater than the wave number of the external media k_2. The corresponding guided waves propagate more slowly along the antennas than plane waves in the medium, and are the slow waves of helical structures. For modes ($n > 0$), the wave numbers can be complex, and were studied in some detail in [5].

Lossy Media: For lossy external medium where $\mathrm{Re}(k_2) > \mathrm{Re}(k_1)$, the propagation constants for the guided modes are found to be complex in general, and their magnitudes are not necessarily greater than the magnitude of the wave number of the external medium. We utilize a numerical method to solve the dispersion equation (10) for the complex propagation constant β_o, under a variety of conditions. The method was based on a modified Newton–Raphson procedure, implemented using Matlab [MathWorks, Inc.]. For lossless external media, the result agree with solutions given in [5].

V. Numerical Results

Fig. 3 presents dispersion diagrams (k-β diagrams) for the $n = 0$ guided modes of the antenna in lossy media. In this figure, the pitch angle is fixed at 15 degrees; the loss tangent $\tan(\gamma) = \varepsilon''/\varepsilon'$ of the outside medium is varied from 0.1 to 0.7.

Fig. 4 shows the propagation constant β_o as a function of helical pitch angle α. Again, the loss tangent of the outside medium is varied, but the frequency is fixed at 915 MHz (a typical frequency used in biomedical applications). The real part of the permittivity of the outside medium was taken to be 30 times greater than that of the inside insulation $\varepsilon_2'/\varepsilon_1' = 30$.

The solutions for the lossy media are quite different from the loss-free case, and in particular reveal two distinct propagating guided modes. One mode, identified in Fig. 3 and 4 as β_{slow}, has a phase velocity less than that of plane waves in the external media and corresponds to a similar slow wave mode found in the lossless case ($\mathrm{Re}(k_1) < \mathrm{Re}(k_2) < \mathrm{Re}(\beta_{\mathrm{slow}})$). Another mode, identified as β_{faster},[1] has a phase velocity greater than that of plane waves in the external media, but less than that of the inside dielectric ($\mathrm{Re}(k_1) < \mathrm{Re}(\beta_{\mathrm{faster}}) < \mathrm{Re}(k_2)$). It appears that this guided mode can only exist if the outside medium has loss, and consequently, to the best of our knowledge, has not been reported in previous studies of helical antennas radiating into free space.

The effect of varying the loss of the outside medium can be seen in Fig. 3 and 4. Clearly, as the loss tangent increases, only the attenuation constant of the slow wave is significantly affected.

[1]The term faster mode generally refers to modes with phase velocities greater than that of the internal and external medium. Here, we use the term faster mode to refer to modes with phase velocities greater than that of plane wave propagation in the external medium, but less than in the internal medium.

VI. Effect of Feedpoint and Termination

The above results describe the characteristics of guided waves that can propagate along an infinitely long helical sheath structure. However, it is necessary to account for the terminations of the helical antenna which, for present purposes, consist of a coaxial feedpoint at one end and a short circuit at the other.

The effect of these terminations can be modeled by expanding the given source fields on an orthogonal basis using orthogonality relations that can be obtained for modes in the helical sheath model. We present, here, such orthogonality relations for the helical sheath. This specific analysis follows from a more general analysis given by McIsaac [14].

Orthogonality Relations

Consider any two different modes, viz., mth and nth modes, propagating in the helical sheath. The Lorentz reciprocity theorem is used to relate them by

$$(\beta_n+\beta_m)\int_{\rho=a}^{\infty}\int_{\phi=0}^{2\pi}\Big[\tilde{E}_n(\rho,\phi)\times\tilde{H}_m(\rho,\phi) - \tilde{E}_m(\rho,\phi)\times\tilde{H}_n(\rho,\phi)\Big]\cdot\hat{a}_z\rho\,d\phi\,d\rho=0. \quad (11)$$

For those modes in which $\beta_n=-\beta_m$, the above integral may obtain a nonzero value.

In general, for a bidirectional reciprocal waveguide, the electric and magnetic fields of an arbitrary source (represented by superscript s) at location z can be expanded into an infinite sum of forward and backward traveling guided modes (represented by superscripts $+$ and $-$, respectively) and a continuous set of radiation modes:

$$\tilde{E}^s(\rho,\phi,z)=\sum_{n=-\infty}^{\infty}\sum_{p=1}^{N}\Big(a_{n,p}\tilde{E}^+_{n,p}(\rho,\phi)e^{-j\beta^+_{n,p}z} + b_{n,p}\tilde{E}^-_{n,p}(\rho,\phi)e^{-j\beta^-_{n,p}z}\Big) + \text{Radiation modes} \quad (12)$$

$$\tilde{H}^s(\rho,\phi,z)=\sum_{n=-\infty}^{\infty}\sum_{p=1}^{N}\Big(a_{n,p}\tilde{H}^+_{n,p}(\rho,\phi)e^{-j\beta^+_{n,p}z} + b_{n,p}\tilde{H}^-_{n,p}(\rho,\phi)e^{-j\beta^-_{n,p}z}\Big). + \text{Radiation modes} \quad (13)$$

Since we are interested in the heating characteristics seen near the surface of the helical antennas, the radiation modes, which contribute primarily to the antenna's far field, are not included in this analysis. For our helical sheath case, where we take only $n=0$ guided modes and ignore the radiation modes, (12) and (13) reduce to

$$\tilde{E}^s(\rho,z)\approx\sum_{p=1}^{N}\Big(a_p\tilde{E}^+_p(\rho)e^{-j\beta^+_p z}+b_p\tilde{E}^-_p(\rho)e^{-j\beta^-_p z}\Big) \quad (14)$$

$$\tilde{H}^s(\rho,z)\approx\sum_{p=1}^{N}\Big(a_p\tilde{H}^+_p(\rho)e^{-j\beta^+_p z}+b_p\tilde{H}^-_p(\rho)e^{-j\beta^-_p z}\Big) \quad (15)$$

where the subscript $n=0$ has been omitted for convenience, and the ϕ dependance removed to illustrate that only those modes independent of azimuthal variation are being considered.

The unknown coefficients a_p and b_p are obtained by applying the Lorentz reciprocity theorem (11) to (14) and (15). This results in the following expressions for a_p and b_p, as given by McIsaac [14]:

$$e^{-j\beta^+_p z}a_p=\frac{\int_a^{\infty}\Big[\tilde{E}^-_p\times\tilde{H}^s-\tilde{E}^s\times\tilde{H}^-_p\Big]\cdot\hat{a}_z\rho\,d\rho}{\int_a^{\infty}\Big[\tilde{E}^-_p\times\tilde{H}^+_p-\tilde{E}^+_p\times\tilde{H}^-_p\Big]\cdot\hat{a}_z\rho\,d\rho} \quad (16)$$

$$e^{-j\beta^-_p z}b_p=\frac{-\int_a^{\infty}\Big[\tilde{E}^+_p\times\tilde{H}^s-\tilde{E}^s\times\tilde{H}^+_p\Big]\cdot\hat{a}_z\rho\,d\rho}{\int_a^{\infty}\Big[\tilde{E}^-_p\times\tilde{H}^+_p-\tilde{E}^+_p\times\tilde{H}^-_p\Big]\cdot\hat{a}_z\rho\,d\rho}. \quad (17)$$

Equations (16) and (17) are valid for any reciprocal waveguide. If possible, it is convenient to express these relations only in terms of the forward traveling modes and source field. For the case of the sheath helix, this can be accomplished by noting the relationship between the propagation constant and field components of the forward and backward traveling waves given as

$$\beta^-_o=-\beta^+_0,\quad E^-_\rho=-E^+_\rho,\quad E^-_\varphi=E^+_\phi,\quad E^-_z=E^+_z,$$
$$H^-_\rho=-H^+_\rho,\quad H^-_\phi=H^+_\phi\quad\text{and}\quad H^-_z=H^+_z.$$

Substituting these equalities into (16) and (17) results in the following expansion coefficients a_p and b_p for the sheath helix:

$$e^{-j\beta_p z}a_p=\frac{-\int_a^{\infty}\Big(E^+_{\rho,p}H^s_\phi+E^+_{\phi,p}H^s_\rho+E^s_\rho H^+_{\phi,\rho}+E^s_\phi H^+_{\rho,p}\Big)\rho\,d\rho}{2\int_a^{\infty}\Big(E^+_{\rho,p}H^+_{\phi,p}+E^+_{\phi,p}H^+_{\rho,p}\Big)\rho\,d\rho} \quad (18)$$

$$e^{+j\beta_p z}b_p=\frac{\int_a^{\infty}\Big(E^+_{\rho,p}H^s_\phi-E^+_{\phi,p}H^s_\rho-E^s_\rho H^+_{\phi,\rho}+E^s_\phi H^+_{\rho,p}\Big)\rho\,d\rho}{2\int_a^{\infty}\Big(E^+_{\rho,p}H^+_{\phi,p}+E^+_{\phi,p}H^+_{\rho,p}\Big)\rho\,d\rho}. \quad (19)$$

where E^s and H^s refer to the known source fields at z, $E^+_{\rho,p}$, $E^+_{\phi,p}$, $H^+_{\rho,p}$, $H^+_{\phi,p}$, and $E^-_{\rho,p}$, $E^-_{\phi,p}$, $H^-_{\rho,p}$ and $H^-_{\phi,p}$ are the transverse field components of the forward and backward traveling waves, respectively.

Introduction of the Feedpoint from the Coaxial Source

We assume that the helical antennas are driven by a coaxial line source. In considering the source field distribution, we ignore higher order modes in the coaxial cable, and we also use normalized electric and magnetic fields. At the feedpoint of the antenna $z=0$ (i.e., the junction of the antenna with the inner conductor of the coaxial line), the normalized electric and magnetic field distributions are assumed to be

$$\begin{array}{llll} E^s_\rho=\frac{1}{\rho} & H^s_\phi=\sqrt{\frac{\epsilon_r}{\mu_o}}\frac{1}{\rho} & a<\rho<b \\ E^s_\rho=0 & H^s_\rho=0 & \rho>b. \end{array} \quad (20)$$

Assuming that the waveguide is infinitely long, contribution of the coaxial source at $z = 0$ to the forward traveling modes can be expressed as

$$\tilde{E}^s(\rho, z=0) \approx \sum_{p=1}^{N} a_p \tilde{E}_p^+(\rho)$$
$$\tilde{H}^s(\rho, z=0) \approx \sum_{p=1}^{N} a_p \tilde{H}_p^+(\rho). \quad (21)$$

To obtain the unknown coefficients, a_p, we substitute the electric and magnetic fields from the coaxial source (20) into the orthogonality relation (18). This results in

$$a_p = \frac{-\int_a^b \left(E_{\rho,p}^+ \sqrt{\frac{\epsilon_1}{\mu_o}} + H_{\phi,p}^+\right) d\rho}{2\int_a^\infty \left(E_{\rho,p}^+ H_{\phi,p}^+ + E_{\phi,p}^+ H_{p\rho,}^+\right) \rho\, d\rho}. \quad (22)$$

Introduction of a Short Circuit Termination

The antennas are shorted at the distal end ($z = L$), where the helix is connected to the inner line of the coaxial cable. The reflections from this short circuit termination can also be included in the model. For simplicity, we assume that only a single reflection occurs at the end of the antenna, and that the reflected wave does not significantly disturb the source fields at $z = 0$. In a lossy external medium, this is justified due to the rapid attenuation of both forward and reflected waves along the antenna.

Since we model the short circuit termination as a perfectly conducting cap at $z = L$, the sum of the forward and reflected waves must then satisfy the condition that the total tangential electric field vanishes at this termination. To satisfy this condition, the tangential component of electric field for the reflected wave must be related to the incident wave at $z = L$ by

$$\tilde{E}_t^- = E_\rho^- \hat{\rho} + E_\phi^- \hat{\phi} = -E_\rho^+ \hat{\rho} - E_\phi^+ \hat{\phi} \quad (23)$$

where superscripts $-$ and $+$ refer again to the reflected and incident traveling waves, respectively, and subscript t denotes the tangential component of electric field. Since this effectively means that the reflection coefficient at $z = L$ is essentially unity, the tangential component of magnetic field, of the reflected wave, is related to those of the forward traveling wave as

$$\tilde{H}_t^- = H_\rho^- \hat{\rho} + H_\phi^- \hat{\phi} = H_\rho^+ \hat{\rho} + H_\phi^+ \hat{\phi}. \quad (24)$$

The total reflected wave at $z = L$, denoted by subscript *tot*, defined in (23) and (24), can also be expanded into a sum of the $n = 0$ propagating modes. However, in this case, we choose the expansion in terms of modes propagating in the $-z$ direction. Hence,

$$\tilde{E}_{tot}^-(\rho) \approx \sum_{p=1}^{N} b_p \tilde{E}_p^-(\rho) e^{-j\beta_p^- z}$$
$$\tilde{H}_{tot}^-(\rho) \approx \sum_{p=1}^{N} b_p \tilde{H}_p^-(\rho) e^{-j\beta_p^- z}. \quad (25)$$

The total reflected electric and magnetic fields at $z = L$ are obtained by substituting (22) into (21), replacing z by L, and using (23) and (24). Thus,

$$\tilde{E}_{tot}^-(\rho, L) = \sum_{p=1}^{N} \frac{\int_a^b \left(E_{\rho,p}^+ \sqrt{\frac{\epsilon_1}{\mu_o}} + H_{\phi,p}^+\right) d\rho}{2\int_a^\infty \left(E_{\rho,p}^+ H_{\phi,p}^+ + E_{\phi,p}^+ H_{\rho,p}^+\right) \rho\, d\rho} \cdot \tilde{E}_p^+(\rho) e^{-j\beta_p^+ L} \quad (26)$$

$$\tilde{H}_{tot}^-(\rho, L) = \sum_{p=1}^{N} \frac{-\int_a^b \left(E_{\rho,p}^+ \sqrt{\frac{\epsilon_1}{\mu_o}} + H_{\phi,p}^+\right) d\rho}{2\int_a^\infty \left(E_{\rho,p}^+ H_{\phi,p}^+ + E_{\phi,p}^+ H_{\rho,p}^+\right) \rho\, d\rho} \cdot \tilde{H}_p^+(\rho) e^{-j\beta_p^+ L}. \quad (27)$$

The unknown coefficients, b_p, for the reflected wave can now be obtained by applying (23)–(27) to the orthogonality relation (19), and are given as (see (28) at the bottom of the page) where the terms which contain subscript *tot* refer to the field components defined in (26) and (27). The total reflected wave is now obtained by substituting (28) into (25).

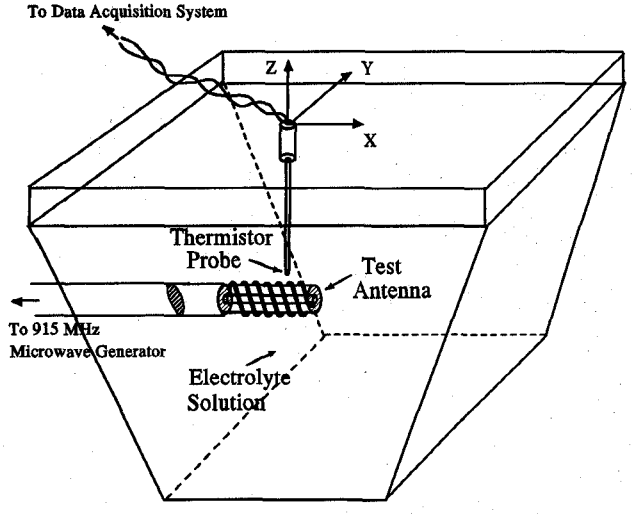

Fig. 5. SAR mapping apparatus. Thermistor probe is translated about the test antenna, and records local specific absorption rate in bath of electrolyte solution.

$$b_p e^{-j\beta_p^- L} = \frac{\int_a^\infty \left(E_{\rho,p}^- H_{\phi,tot}^- + E_{\phi,p}^- H_{\rho,tot}^- + E_{\rho,tot}^- H_{\phi,p}^- + E_{\phi,tot}^- H_{\rho,p}^-\right) \rho\, d\rho}{2\int_a^\infty \left(E_{\rho,p}^- H_{\phi,p}^- + E_{\phi,p}^- H_{\rho,p}^-\right) \rho\, d\rho} \quad (28)$$

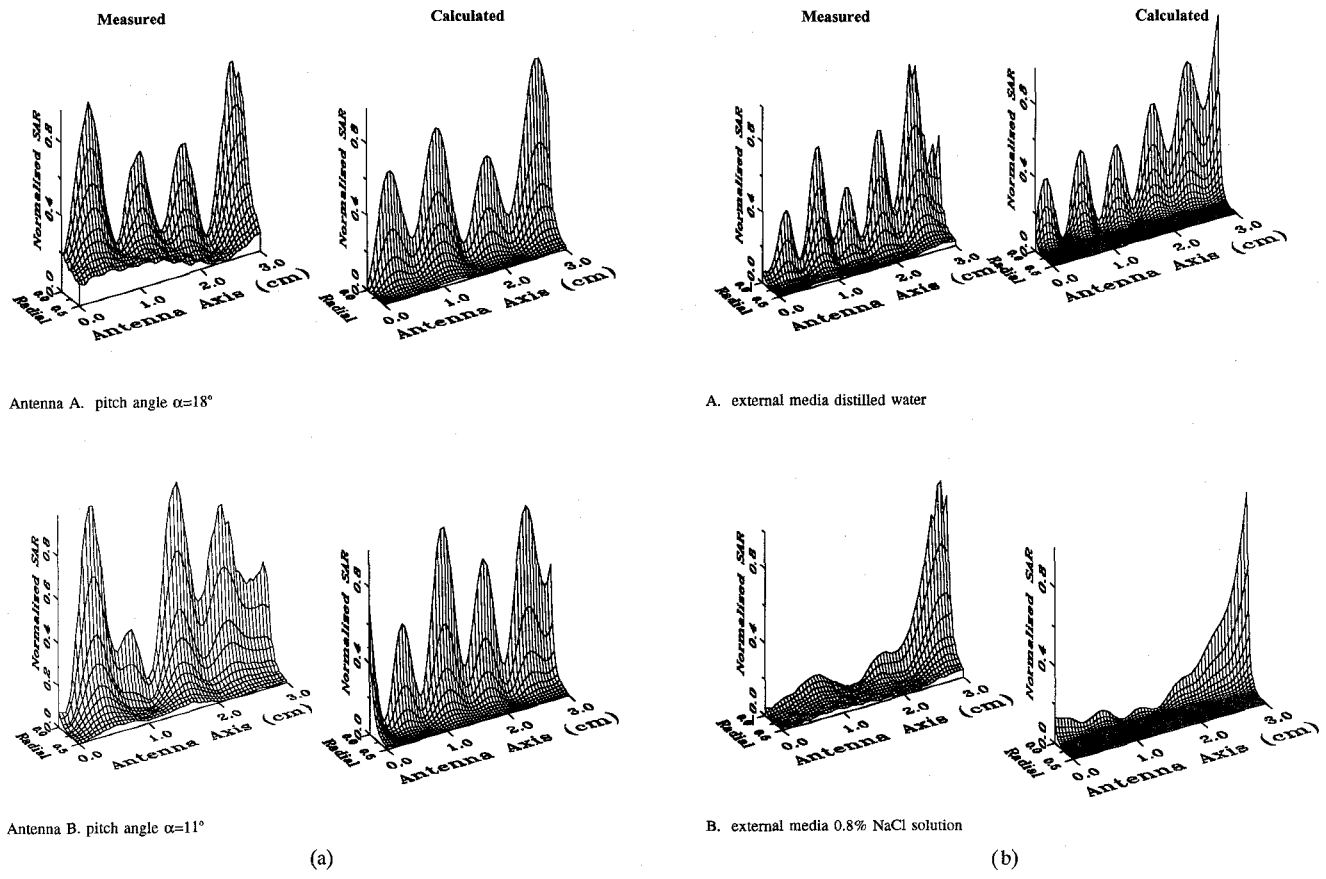

Fig. 6. (a) Measured and calculated normalized SAR patterns for helical antennas immersed in distilled water and driven by a 30 Watt, 915 MHz generator. The antenna length is $L = 3.0$ cm, inner radius, $a = .03$ cm, outer radius, $b = 0.1$ cm. Inside dielectric is teflon with $\varepsilon_1 = 2.1$. Helical pitch angles: Antenna A $\alpha = 18°$; Antenna B $\alpha = 11°$.(b) Measured and calculated normalized SAR patterns for helical antennas immersed in various concentrations of NaCl electrolyte, and driven by a 30 Watt, 915 MHz generator. The antenna length is, $L = 3.0$ cm, inner radius, $a = 0.03$ cm, outer radius, $b = 0.1$ cm. Inside dielectric is teflon with $\varepsilon_1 = 2.1$ and the helical pitch angle, $\alpha = 11°$.

VII. Total Electric and Magnetic Fields

After including the coaxial line source and the short circuit termination, the total electric and magnetic fields are obtained as the sum of forward plus reflected modes as

$$\tilde{E}_{tot} = \tilde{E}^{+}_{tot} + \tilde{E}^{-}_{tot} = \sum_{p=1}^{N} \left(a_p \tilde{E}^{+}_{p} e^{-j\beta^{+}_{p} z} + b_p \tilde{E}^{-}_{p} e^{-j\beta^{-}_{p} z} \right) \tag{29}$$

$$\tilde{H}_{tot} = \tilde{H}^{+}_{tot} + \tilde{H}^{-}_{tot} = \sum_{p=1}^{N} \left(a_p \tilde{H}^{+}_{p} e^{-j\beta^{+}_{p} z} + b_p \tilde{H}^{-}_{p} e^{-j\beta^{-}_{p} z} \right) \tag{30}$$

where the coefficients a_p and b_p are given by (22) and (28), respectively. The quantity of interest here is the specific absorption rate (SAR) which is now given as

$$\text{SAR} = \frac{1}{2\rho} \sigma \left| \tilde{E}_{tot} \right|^2 \frac{W}{Kg} \tag{31}$$

where σ and ρ are the conductivity and density of the outside medium, respectively.

VIII. Experimental Studies

The antenna SAR patterns were experimentally measured using the computer-controlled apparatus shown in Fig. 5. The antennas consisted of helices 0.2 cm in diameter and length ranging from 3.0 to 15.0 cm, mounted on standard semirigid coaxial line. The helices were wound using precision spring-winding facilities at Arrow International (Reading, PA).

The antenna was mounted in a tank filled with aqueous electrolyte of varying conductivity. The probe consisted of a small thermistor, 0.25 mm in diameter, encased in a glass micropipette, whose thermal response time was less than 0.1 s. The leads of the thermistor were a twisted pair of shielded wires, aligned perpendicularly to the field of the antenna. This arrangement was found to be sufficiently immune from interference to permit accurate measurements of the antenna SAR pattern. The probe was mounted on a translating platform, controlled by stepping motors. The entire measurement process, including movement of the probe and recording and analysis of the output of the thermistor, was controlled by a laboratory computer (Hewlett-Packard Vectra) running ASYST.

To measure the SAR pattern, the transient temperature increase in the outside medium was measured following a short pulse (0.5 s) from a 30-W 915-MHz microwave transmitter. In other experiments, we have established that convective fluid

flow requires longer periods (several seconds) to develop; thus, the probe records the local rate of heating (and, hence, the local SAR) uncontaminated by artifact from fluid convection. Using this apparatus, the three-dimensional SAR pattern of an antenna could be mapped with a spatial resolution of 0.5 mm, over a total time period of a few hours.

IX. Experimental Results

In Fig. 6(a), the measured normalized SAR patterns with two different helical pitch angles ($\alpha = 11°$, and $20°$) in distilled water are compared to the calculated SAR patterns. In Fig. 6(b), the normalized SAR pattern for one of the antennas ($\alpha = 11°$) in electrolyte solutions of increasing conductivity are compared to the calculated SAR.

The calculated and measured results show a distinct standing wave pattern along the length of the antenna, whose wave number depends strongly on the helical pitch angle. As the conductivity of the external medium increases, the heating pattern shifts toward the antenna's tip. This results in a highly nonuniform heating pattern, which is unattractive for the present application of catheter ablation. We will show, in a subsequent paper, that the addition of a thin layer of insulation around the outside of the helical structure can produce a more uniform heating pattern.

X. Input Impedance

To gain a deeper understanding of the heating characteristics of the helical antenna, it is necessary to consider the input impedance also. In Fig. 7, the measured resistive and reactive components of the input impedance are plotted as a function of frequency. The outside medium was 0.8% saline, and antennas with helical pitch angles varying from 4° to 15° were measured. The results show an insensitivity of input impedance with changes in helical pitch angle. This most likely reflects the contribution of the fast wave which is also rather insensitive to variations in helical pitch angle.

Unfortunately, the helical sheath model could not adequately predict the measured input impedance. This is not surprising, since the input impedance is far more sensitive to current distribution near the feedpoint and to angular variations in electric field than the SAR pattern. The present helical sheath model assumes no variations with respect to ϕ. Moreover, higher order modes, which were not considered, could significantly affect the input impedance. In order to reasonably predict the input impedance, the helical sheath model should probably be replaced by a more realistic (and complicated) model such as a helical tape model.

XI. Discussion

There is clearly a good agreement between the antenna field patterns that are predicted by the model, and the experimental results. For these antennas, the antenna current (and hence SAR distribution in the medium) strongly reflects the presence of standing waves along the antenna. These patterns are strongly sensitive to the helical pitch; a tighter helix results in a lower propagation constant and tighter standing

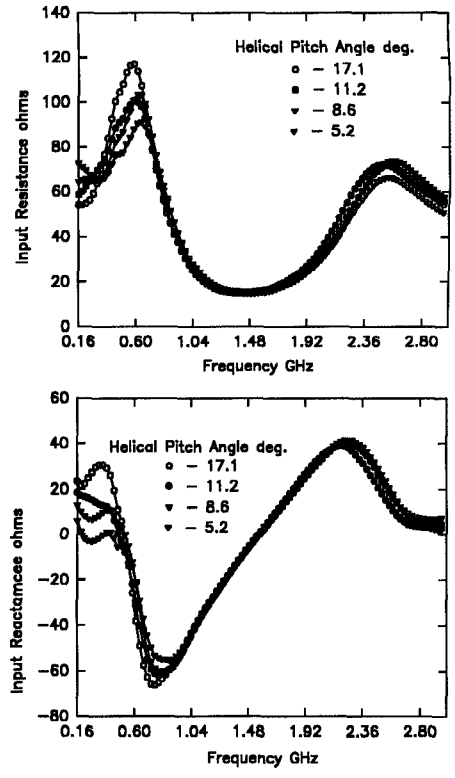

Fig. 7. Input Impedance vs. frequency for 3.0 cm long helical antennas of various pitch angles immersed in 0.8% (wt/wt) NaCl. Inner radius, $a = 0.03$ cm, outer radius, $b = 0.1$ cm.

wave pattern. Prolonged heating will lead to a more diffuse heating distribution than shown here due to the effects of heat conduction and convection.

Another prominent feature is the high sensitivity of the antenna SAR pattern to the conductivity of the medium. This results from the fact that one mode is much more strongly damped than the other, and essentially vanishes for media that are very lossy. For the proposed biomedical applications, this will result in an antenna which heats predominantly at its distal tip. We will show, in a subsequent contribution, that this effect is much less pronounced in helical antennas covered by a thin layer of insulation. This result will be reported shortly.

These feature have significant implications for the prospective biomedical application of such antennas. Clearly, the depth of heating is very limited and far less than that of a simple dipole of comparable dimensions [15]. On the other hand, helical antennas can be designed that have a greater uniformity of heating along their length when they are covered by a layer of insulation. For applications (such as hyperthermia) where the goal is to achieve the greatest depth of heating, dipole antennas are obviously preferable. For catheter ablation or angioplasty applications of depth of heating is often neither required nor desirable, and helical antennas might be preferable.

Acknowledgment

We thank Microwave Medical Systems, Inc., Littleton, MA, for generous support of this study.

REFERENCES

[1] M. S. Mirotznik, D. K. Bogen, and K. R. Foster, "Spiraled-helix antenna for catheter ablation of myocardial tissue using microwave energy," in *Proc. 16th Northeast Bioeng. Conf.,* State College, PA, Mar. 1990.

[2] T. Satoh, P. R. Stauffer, and J. R. Fike, "Thermal distribution studies of helical coil microwave antennas for interstitial hyperthermia," *J. Rad. Oncol. Biol. Phys.,* vol. 15, pp. 1209–1218, 1988.

[3] T. Satoh *et al.,* "Interstitial helical coil microwave antenna for experimental brain hyperthermia," *Neurosurgery,* vol. 23, pp. 564–569 (1988).

[4] A. Wu *et al.,* "Performance characteristics of a helical microwave interstitial antenna for local hyperthermia," *Health Phys.,* vol. 14, pp. 235–237, 1987.

[5] S. Sensiper, "Electromagnetic wave propagation on helical conductors," *Proc. IRE,* vol. 2, pp. 149–161, 1955.

[6] A. R. Neureuther, P. W. Klock, and R. Mittra, "A study of the sheath helix with a conducting core and its application to the helical antenna," *IEEE Trans. Antennas Propagat.* vol. AP-15, pp. 203–208, 1967.

[7] J. Perini, "A side-fire helical antenna," General Electric, Electronics Park, Syracuse, NY, Tech. Rep. R61EB1, Oct. 1961.

[8] D. A. Hill and J. R. Wait, "Propagation along a coaxial cable with a helical shield," *IEEE Trans. Microwave Theory Tech.,* vol. 28, pp. 84–89, 1990.

[9] C. L. Chen, "Infinite helical sheath antenna," *Radio, Sci.,* vol. 1, pp. 589–600, 1966.

[10] J. P. Casey and R. Bansal, "Finite length helical sheath antenna in a general homogenous medium," *Radio Sci.,* vol. 23, pp. 1141–1151, 1988.

[11] R. Hines *et al.,* "Microwave applicator/receiver apparatus," U.S. patent 4,583,556, Apr. 22, 1986.

[12] K. S. H. Lee and C. E. Baum, "Applications of modal analysis to braided wire shields," *IEEE Trans. Electromagn. Compat.,* vol. EMC-17, p. 159–169, 1975.

[13] J. A. Staratton, *Electromagnetic Theory.* New York: McGraw-Hill, 1941.

[14] P. R. McIsaac, "Mode orthogonality in reciprocal and nonreciprocal waveguides," *IEEE Trans. Microwave Theory Tech.,* vol. 39, pp. 1808–1816, 1991.

[15] R. W. King, B. S. Trembly, and J. W. Stohbehn, "The electromagnetic field of an insulated antenna in a conducting or dielectric medium," *IEEE Trans. Microwave Theory Tech.,* vol. MTT-31, pp. 574–583, 1983.

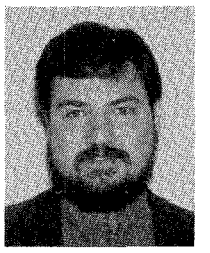

Mark S. Mirotznik (M'92) was born in Sycamore, IL, in 1965. He received a B.S. in electrical engineering from Bradley University, Peoria IL, in 1965. He received a M.S. in electrical engineering, a M.S. in biomedical engineering and a Ph.D. in biomedical engineering all from the University of Pennsylvania in 1991 and 1992 resepctively.

Upon graduation he joined the electrical engineering faculty at The Catholic University of America as an assistant professor. His current research interests are in catheter ablation of the heart and medical imaging.

Nader Engheta (S'81–M'82–SM'89), photograph and biography not available at the time of publication.

Kenneth R. Foster, photograph and biography not available at the time of publication.